Journal of MATERIALS RESEARCH

Article
DOI: 10.1557/jmr.2020.26

A systematic investigation on physical properties of spray pyrolysis–fabricated CdS thin films for opto-nonlinear applications: An effect of Na doping

M. Aslam Manthrammel[1], Mohd. Shkir[1,a], S. Shafik[2], Mohd. Anis[3], S. AlFaify[1,b]

[1]Research Center for Advanced Materials Science (RCAMS), King Khalid University, Abha 61413, Saudi Arabia; and Advanced Functional Materials & Optoelectronics Laboratory (AFMOL), Department of Physics, Faculty of Science, King Khalid University, Abha 61413, Saudi Arabia
[2]Thin Film Physics Laboratory, Department of Physics, Electronics and Photonics, Rajarshi Shahu Mahavidyalaya, Latur, Maharashtra 413512, India
[3]Department of Physics and Electronics, Maulana Azad College of Arts, Science and Commerce, Aurangabad,, Maharashtra 431001, India
[a]Address all correspondence to these authors. e-mail: shkirphysics@gmail.com
[b]e-mail: salfaify@kku.edu.sa

Received: 23 October 2019; accepted: 10 January 2020

The present work investigates the influence of sodium doping on structural, morphological, photoluminescence, linear, nonlinear (NL), and optical limiting (OL) parameters of $Na_xCd_{1-x}S$ thin films (where x = 0.0, 0.5, 1.0, 2.5, and 5.0 wt%) deposited on glass substrates using spray pyrolysis route. X-ray diffraction and Raman analyses confirmed the hexagonal polycrystalline nature of films. Crystallite sizes were decreased from 30 to 17 nm with doping. Scanning electron microscopy (SEM) micrographs also confirmed the nanocrystalline spherical growth. Energy dispersive X-ray spectroscopy (EDS) and SEM mapping studies revealed the presence and homogeneous distribution of individual elements. Transmission of films is found to lie between 45 and 60%. Although the low doping caused the reduction of the effective band gap, higher doping caused a blue shift in band gap, with an associated reduction in crystallite sizes. The refractive index values are found within 1–2 in visible and their maximum values (in range 2.65–3.16) are observed at 2500 nm. Photoluminescence (PL) spectra showed broad emission peak at ~520 ± 10 nm. Dielectric and NL analyses were also carried out. OL results were promising for the systematic gradual decrease of intensity from 100 to 72%, with doping for power regulating applications.

Introduction

In recent years, much attention has been devoted to the CdS-based semiconductor thin film industry because of the various unique potential characteristics they owe. They have been found to be useful in sustained energy harvesting and many other environmental and optoelectronic applications. CdS is best known for its n-type wide band gap of 2.4 eV that makes it a suitable window layer counterpart for the solar cell applications in conjunction with the p-type semiconductor absorber thin films like CdTe, $CuInSe_2$, Cu_2ZnSnS_4 (CZTS), or Cu $(In_{1-x}Ga_x)$ Se_2 (CIGS) [1, 2, 3]. Recently, it has been found useful as the electron-conducting layer in perovskite solar cells [4]. The other applications are not limited to light-emitting diodes, laser, photocatalysis, field-effect transistors, photosensor, etc. [5, 6, 7, 8, 9, 10]. CdS thin films have been deposited using numerous physical and chemical deposition techniques. Few of them are sputtering, molecular beam epitaxy, thermal evaporation, chemical bath deposition, successive ionic layer adsorption and reaction, spray pyrolysis, and electrodeposition [11, 12]. Among them, spray pyrolysis is a simple and cost-effective process to produce uniform and high-quality thin films without the requirement of high vacuum equipment. The technique yields nearly uniform and high-quality thin films and supports large-scale coating and even substrates with complex geometries [13, 14]. Many attempts have been done to alter the structural, electrical, and optical properties of the CdS thin films to improve them in view of device-oriented applications [15, 16, 17]. The invention of nanotechnology has brought many opportunities to vary the semiconductor characteristics by growing them in nanoscale having different structures and morphologies. Doping with suitable material is another important criterion adopted in this field for material property variation. In the literature, CdS has been doped with a variety of materials including rare earth

materials such as La, Y, Gd, and Er and metals such as Al, In, Cu, and Au [12, 18, 19, 20, 21, 22, 23]. However, very few literature exist on Na-doped CdS thin films, and the existing works did not explore a comprehensive idea on the effect of doping variation on the structural, optical, and nonlinear (NL) properties of CdS thin films [24, 25]. In view of these, our attempt is to grow CdS thin films using the spray pyrolysis method in nanoscale with different doping levels of sodium (Na).

Results and discussions

Structural and vibrational spectroscopy studies

X-ray diffraction (XRD) spectra of $Na_xCd_{1-x}S$ films on the glass substrates are shown in Fig. 1(a). The prominent peaks for the samples are marked in the figure with their corresponding diffraction planes. The interplanar distance and the peaks are in accordance with the standard diffraction spectra of hexagonal CdS and matches with the ICDD card no. 41-1049. It can be realized from the figure that the broadness of the peaks increases with increase in sodium content, indicating a clear decrease in crystallite size with the concentration. Also, it is noted that the (002), (101), (103), and (112) planes also match with the hexagonal sodium structure corresponding to the ICDD card no. 01-089-4082, with the planes (100), (002), (110), and (103) indicating the probable presence of sodium in the lattice. Scherer formula [26],

$$D = 0.9\lambda/(\beta\ \cos(\theta)) \quad , \tag{1}$$

was used to assess the crystallite sizes (D) of the samples from the XRD data [27, 28] and arranged in Table I. The dislocation density of the samples which gives the number of dislocations present in the unit area of the sample [29] and microstrain values can be estimated using [30].

$$\delta = 1/D^2 \quad , \tag{2}$$

$$\varepsilon = \beta\ \cos(\theta)/4 \quad . \tag{3}$$

The lattice parameters were also calculated from the XRD data [31], and all the results are tabulated in Table I. A clear decrease in the crystallite size as well as an increase in the lattice parameters can be perceived from the table with the increase of sodium percentage.

Vibrational spectra of $Na_xCd_{1-x}S$ thin films were carried out using Raman spectral analysis, in the 1500–100 cm^{-1} range. This study is important in judging the structural purity of the grown samples as the Raman peak positions are unique characteristics of the sample. Two dominant characteristic Raman peaks of wurtzite CdS structure are clearly observed in Fig. 1(b), which are centered at 301.895 and ~603.69 cm^{-1} [32]. The peaks at 300.93 cm^{-1} are of high intensity and are attributed to the vibrations of longitudinal optical phonon (LO) and those at 603.69 cm^{-1} are comparatively weaker and are identified as the overtones [33, 34]. Both the peaks did not express any significant shift in the peak position with the sodium concentration. This is an indication of impurity-free samples having reasonably minor strain and bond distortion inside the lattice. Besides these dominant peaks, the figure also exhibits two other characteristic modes of wurtzite CdS, one having B_2 symmetry at 212 cm^{-1} and the other with E_2 symmetry at 259 cm^{-1} [32, 35]. The study suggests high purity of the synthesized films.

EDS/SEM mapping and morphological studies

Figures 2(a) and 2(b) display EDS spectrum and SEM mapping analyses carried out on 5.0 wt% $Na_xCd_{1-x}S$ films to make the elemental analyses as well as the uniformity of the samples. The study confirmed both the presence of the individual elements (Cd, S, and Na) from the EDS and the homogeneous distribution of the elements in the sample from the SEM mapping studies. In Figs. 2(b), the Cd, S, and Na e-maps are displayed by red [Fig. 2(b_1)], green [Fig. 2(b_2)], and blue [Fig. 2(b_3)] colors, respectively, and all three together are mapped in Fig. 2(b_4). Figure 2(b_4) confirms the homogeneous distribution of all three elements all over the fabricated film.

Morphological analyses of the samples were carried to understand the information regarding shape, size, and arrangement of particles inside the synthesized $Na_xCd_{1-x}S$ thin films, using SEM studies. Figure 3 displays SEM micrographs for 0.5 wt%, 1.0 wt%, 2.5 wt%, and 5.0 wt% $Na_xCd_{1-x}S$ films, respectively. The images show distinct agglomerated spherical nanoparticles in all the figures. However, it is apparent from the figure that the packing density of each agglomerated particles differ with sodium concentration and are found to be increasing with increasing Na doping wt%. This indicates that each cluster contains more particles, and, in other words, particle size decreases with sodium content. This is in agreement with the XRD data. The images also depict a visual transition of the individual particle arrangements within the microstructure after 2.5 wt% Na doping onwards, finally resulting in big clusters having more crystallites at 5 wt% doping.

Linear optical parameters

Absorbance, transmission, and reflectance analyses

Figure 4(a) represents absorbance and (b) transmission and reflectance spectra of $Na_xCd_{1-x}S$ films measured in the wavelength range 220–2500 nm. From the figure, the films display the transparency above 45% in the visible spectrum, ranging from 45 to 60%, after the band edge and also enhancement in the transparency of the film with the doping

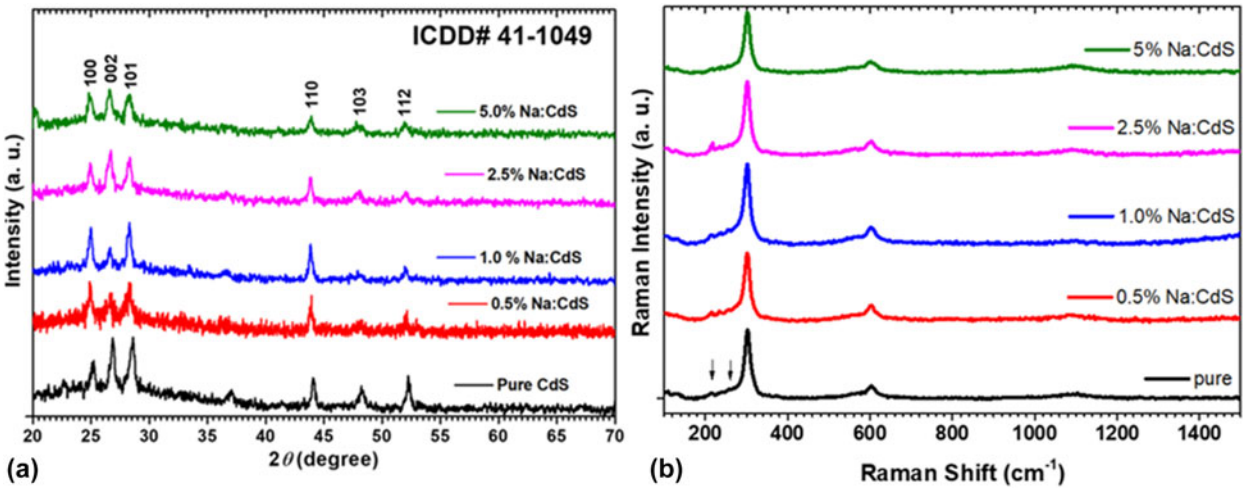

Figure 1: (a) XRD and (b) FT-Raman images of Na-doped (0, 0.5, 1, 2.5, and 5 wt%) CdS films.

TABLE I: Average values of crystallite sizes, dislocation densities, microstrain, and lattice parameters of the $Na_xCd_{1-x}S$ samples estimated from the Scherrer formula.

Sample name	D (nm)	δ (10^{-3} nm^{-2})	ε (10^{-3})	a (Å)	c (Å)	V (Å^3)
0.0 wt% Na	29.14	1.413	4.431	4.085	6.672	111.361
0.5 wt% Na	25.15	1.581	5.338	4.088	6.679	111.461
1.0 wt% Na	22.89	1.997	6.16	4.119	6.726	114.105
2.5 wt% Na	19.12	2.854	7.364	4.119	6.726	114.103
5.0 wt% Na	17.58	3.392	7.968	4.122	6.731	114.366

wt%. This enhancement could be accredited to the decreased crystallite size and the arrangement of particles within the microstructure as evident in Scherer calculations in Table I and SEM micrographs in Fig. 4. It was also noted that the transmission percentage varies with the wavelength as well, and reaches the maximum at around 1700 nm in the IR range and maintains an almost steady state beyond 1700 nm with only a slight decrease in the value. From Figs. 5(a) and 5(b), the band edges of the spectra are observed at 500 ± 3 nm. As evident, the high energy UV region is thoroughly absorbed as it falls above the band edge of the CdS as well as glass substrate. The study also shows the strong dependence of the reflectance spectra with the doping percentage as well as the applied wavelength. The reflectance decreases with the doping wt% below 1450 nm and shows the opposite tendency above 1450 nm wavelength. Thus, the studies indicate that the photovoltaic window layer properties and the IR reflectivity of the CdS thin films could be enhanced by tuning the transparency as well as band gap of the CdS thin films by suitable proportions of sodium doping.

Extinction and refractive indices, and energy gap evaluations

The optical data contain useful information regarding the energy band gap (E_g) and refractive index (n) of the semiconductor material and can be extracted from the absorption coefficient (α which is given by $\alpha = 2.303 \times A/t$, A is the measured absorbance and t is the thickness of film). Also, the extinction coefficient (k) is related to the absorption coefficient with the formula $k = \alpha\lambda/(4\pi)$. The E_g values for the direct allowed transition of the $Na_xCd_{1-x}S$ films can be obtained using Tauc's relation [27, 36, 37, 38, 39, 40, 41, 42, 43, 44].

$$\alpha h\nu = A\left(h\nu - E_g\right)^{1/2} \quad , \tag{4}$$

where $h\nu$ is the energy of the incident photon, and the E_g values correspond to the intercept of linear portion's extrapolation on the $h\nu$ axis in the $(\alpha h\nu)^2$ versus $h\nu$ plot [45]. The "n" values are related to the reflectance "R" data using the Fresnel's formula [46],

$$R = \frac{(n-1)^2 + k^2}{(n+1)^2 + k^2} \quad . \tag{5}$$

Thus "n" can be obtained from the relation,

$$n = \frac{(1+R)}{(1-R)} + \sqrt{\frac{4R}{(1-R)^2} - k^2} \quad . \tag{6}$$

Figure 5(a) shows Tauc's plot for direct transition for the $Na_xCd_{1-x}S$ films. The band gap values are obtained as 2.435, 2.410, 2.398, 2.413, and 2.430 eV for the 0, 0.5, 1, 2.5, and 5 wt% $Na_xCd_{1-x}S$ samples, respectively. It can be seen that the band gap values initially decrease with the Na content, reaches its minimum at 1 wt% doping, and increases above 1 wt% Na doping. This clearly indicates that the effect of small doping quantity of Na on the direct band gap of CdS thin films is to reduce its effective band gap. Similar trend of band gap reduction has been observed with Na doping on ZnO films [47, 48]. However, the increase of Na content also results in

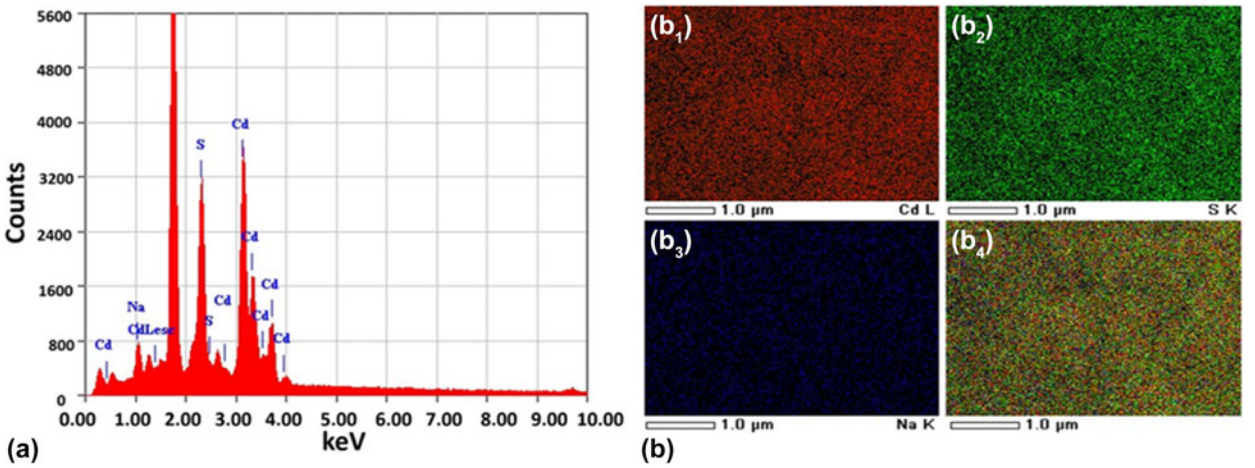

Figure 2: (a) EDS spectrum and (b) SEM mapping images for 5 wt% $Na_xCd_{1-x}S$ films.

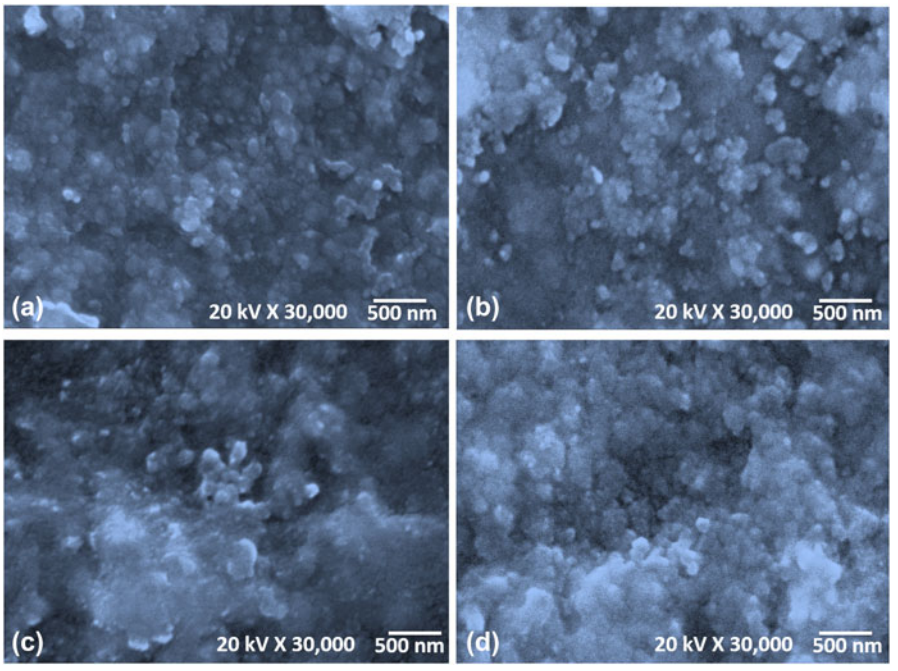

Figure 3: SEM micrographs for (a) 0.5 wt%, (b) 1.0 wt%, (c) 2.5 wt%, and (d) 5.0 wt% $Na_xCd_{1-x}S$ films (with 30,000× magnification).

reducing the crystallite sizes of the samples as evident from Table I and SEM studies. At some point, these two effects might be balancing and the effect of reduced crystallite size on the band gap starts dominating. Thus, the comparative blue shift tendency observed for the 2.5 and 5 wt% samples could be attributed to the decreasing of crystallite sizes with the increase in Na content [49, 50]. Thus, at a higher doping level, Na doping results in the blue shift of the effective band gap. Mageswari et al. also observed this increasing tendency of the CdS band gap with the addition of Na and K in their Na and K dual doping work by chemical bath deposition and attributed to the reduction in crystallite size [24]. At low doping, the Na atoms might be occupying the interstitial sites, whereas at higher doping, they might start to substitute the Cd^{2+} ions. Figures 5(b) and 5(c) represents the plots of refractive index and extinction coefficient for the $Na_xCd_{1-x}S$ films. The refractive index values are found to be decreasing with the doping in the UV-Vis range, and the dependency varies in the IR region. The values are found to be varying between 1 and 2 in the visible range and reaches up to 3.2 for the 0.5 wt% $Na_xCd_{1-x}S$ sample, at 2500 nm. From Fig. 5(c), the extinction coefficient values are found to be varying with the applied wavelength and Na content. The k values have their maximum in the UV range and have steady values after band edge for a wide range of wavelength until 1700 nm and show a slight increase in the values after 1700 nm wavelength.

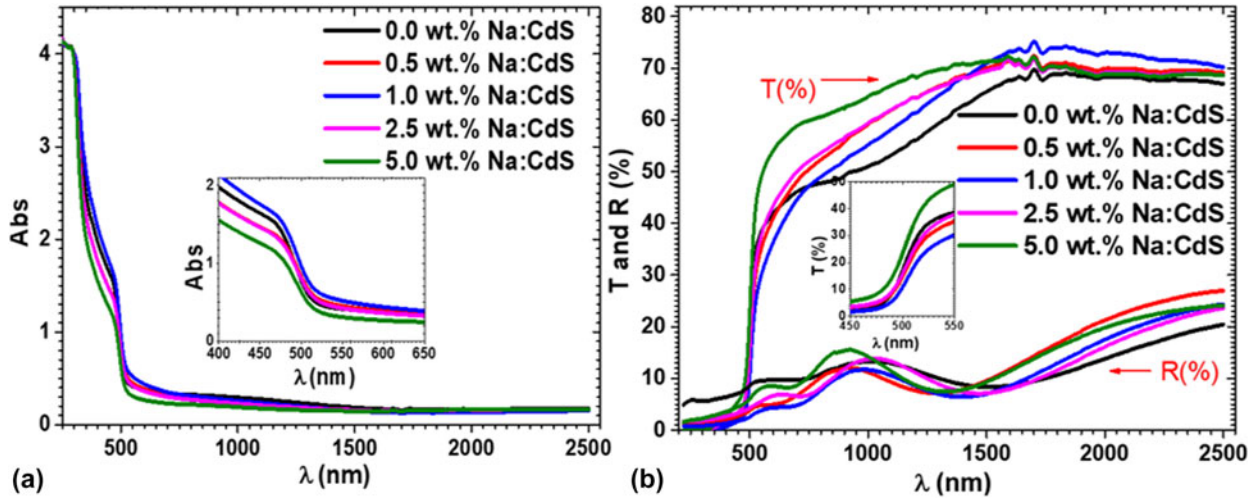

Figure 4: (a) Absorption and (b) transmission and reflectance spectra for $Na_xCd_{1-x}S$ films.

Photoluminescence studies

Pl studies are useful to understand the various transitions occurring inside the sample when light strikes on it. CdS is best known for its broad emission spectra in UV, blue, green, yellow, and red bands arising because of the vacancies of Cd (V_{Cd}) and S (V_s) and interstitial positions of Cd (I_{Cd}) and S (I_s) [51, 52]. These intrinsic defects can act as luminescent centers and cause the broad defect allied PL spectrum [53, 54]. Figures 6(a) and 6(b) represent PL spectra of $Na_xCd_{1-x}S$ thin films excited at 350 and 450 nm, respectively. Both the plots clearly show broad characteristic peaks at around 520 nm for the pure CdS, 530 nm for the 5 wt% $Na_xCd_{1-x}S$ samples, and in between for the intermediate samples, spanning in the green band region. These peaks could be attributed to the band to band emission of the synthesized $Na_xCd_{1-x}S$ samples, and the observed red shift could be attributed to the formation trap levels from sodium atoms inside the energy gap which is moving toward the valence band with the increase in Na concentration which results in an indirect recombination of trap level electrons and the valence band holes [53, 54]. Also, weak bands are observed in the red band range at ~630 and ~675 nm, and might have aroused because of the surface defects caused by Cd vacancy, V_{Cd} [12, 55, 56]. An UV band whose intensity is decreasing with Na doping can be seen at 387 nm from Fig. 6(a), and the reason for the reduction in the intensity could be attributed to the quenching effect from nonradiative recombination [53].

Dielectric constant, loss, and conductivity analyses

Figures 7(a) and 7(b) represent dielectric constant and dielectric loss analyses of the $Na_xCd_{1-x}S$ films. They are the real and imaginary parts of the complex dielectric constant, respectively, and are obtained from the n and k values using the relations [28, 57, 58, 59]:

$$\varepsilon' = n^2 - k^2 \quad , \tag{7}$$

and

$$\varepsilon'' = 2nk \quad . \tag{8}$$

The former is responsible for dispersion and electronic polarization of the electromagnetic wave within the sample and slowdown of its propagation velocity while traveling through the sample. The later could be treated as a measure of rate of disruption of waves in the material as it is associated with the absorption of electric field energy by the dipole motions. From Fig. 7(a), the dielectric constant increases with the applied wavelength except in the range 1000–1500 nm, where it showed the opposite behavior. The high values of dielectric constant at higher wavelengths could be due to the involvement of defect-related conduction process [60]. From Fig. 7(b), the dielectric constant values are higher at the lower wavelengths below the band edge near 500 nm, i.e., at the high energy region of the em spectrum having energies above the band gap. It takes almost steady values until 1700 nm after crossing the band edge regime and increases steadily after 1700 nm. Nevertheless, the dielectric loss values decrease with the increase in Na doping percentage in the wide range of UV-Vis-NIR spectrum.

The optical absorption coefficient (α) data were used to evaluate the electrical and optical conductivities of the $Na_xCd_{1-x}S$ films, using the relations [61, 62].

$$\sigma_{opt} = \alpha nc/4\pi \quad , \tag{9}$$

and

$$\sigma_e = 2\lambda\sigma_{opt}/\alpha \quad , \tag{10}$$

where c is the speed of light.

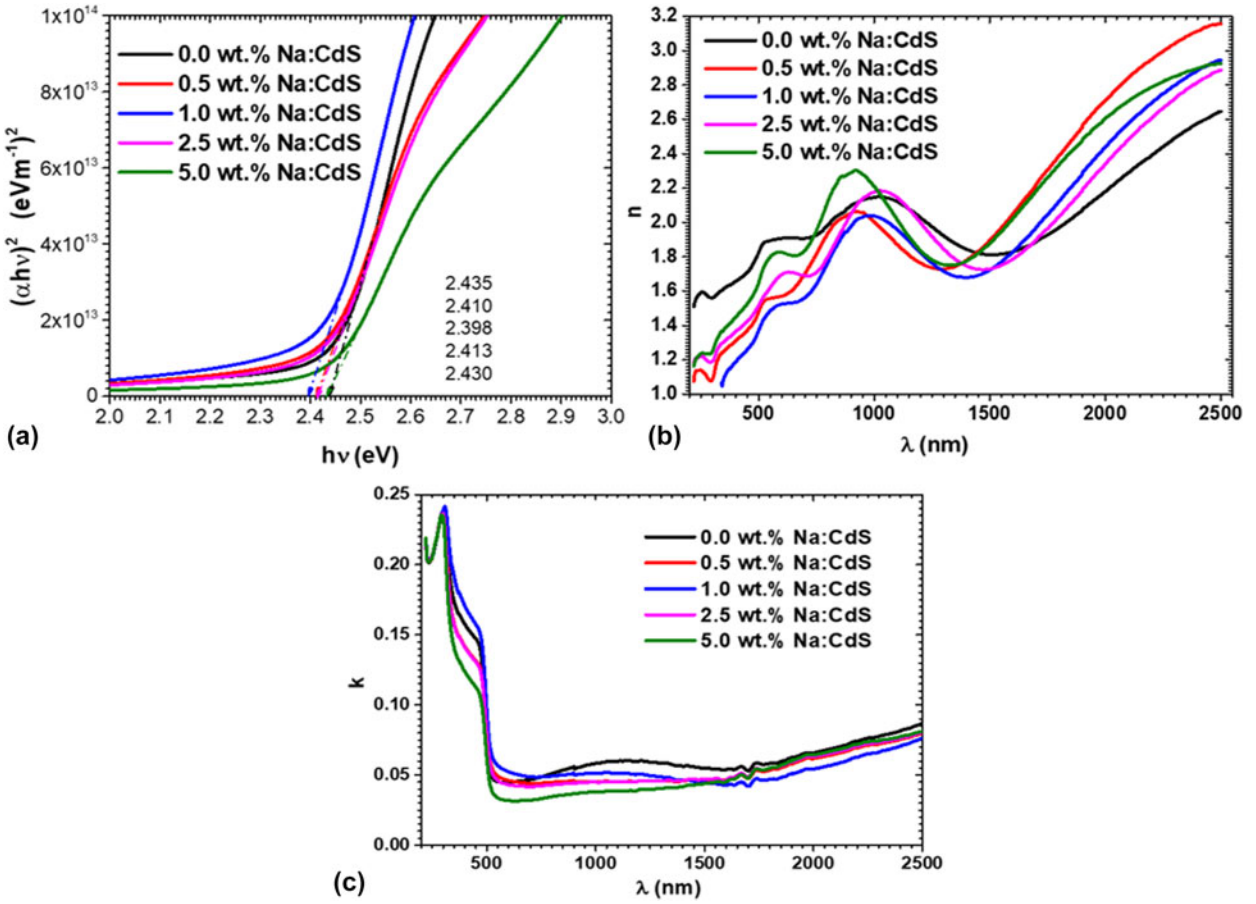

Figure 5: (a) Tauc's plot for direct transition, (b) refractive index, and (c) extinction coefficient for the $Na_xCd_{1-x}S$ films.

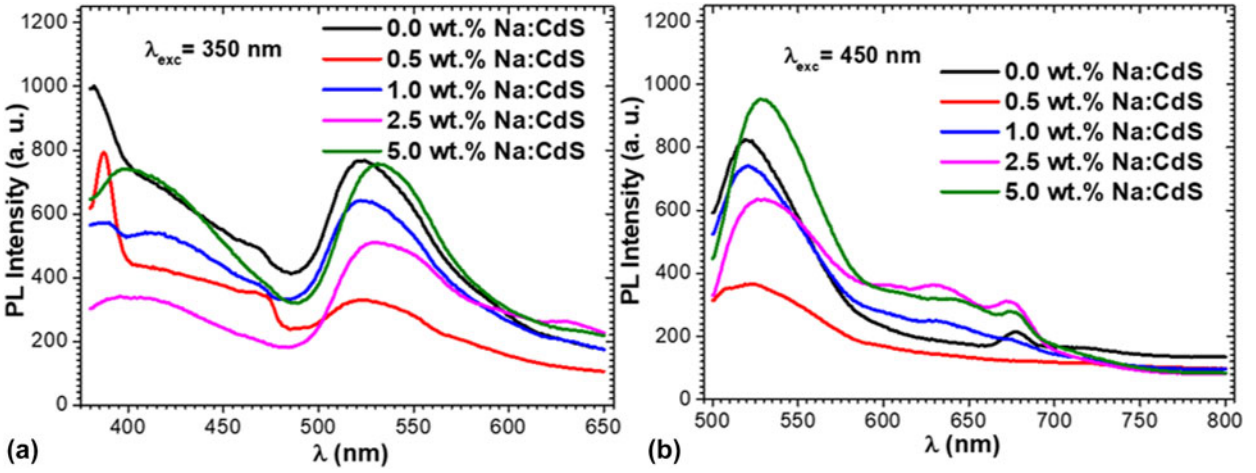

Figure 6: PL spectra of $Na_xCd_{1-x}S$ films excited at (a) 350 nm and (b) 450 nm.

Figures 7(c) and 7(d) represent optical and electrical conductivity plots against wavelength for the different doping levels of $Na_xCd_{1-x}S$ films. As evident, the optical conductivities are highest at the high energy end of the spectrum, especially above band gap energy and below ~500 nm wavelength. After crossing the band edge regime, the optical conductivity values are nearly uniform, and this is in line with previous reports [63]. From the figure, it was also observed that the optical conductivity decreases with the increase of Na wt%. The electrical conductivity plots show a completely different trend with the incident wavelength. As the wavelength increases, the electrical

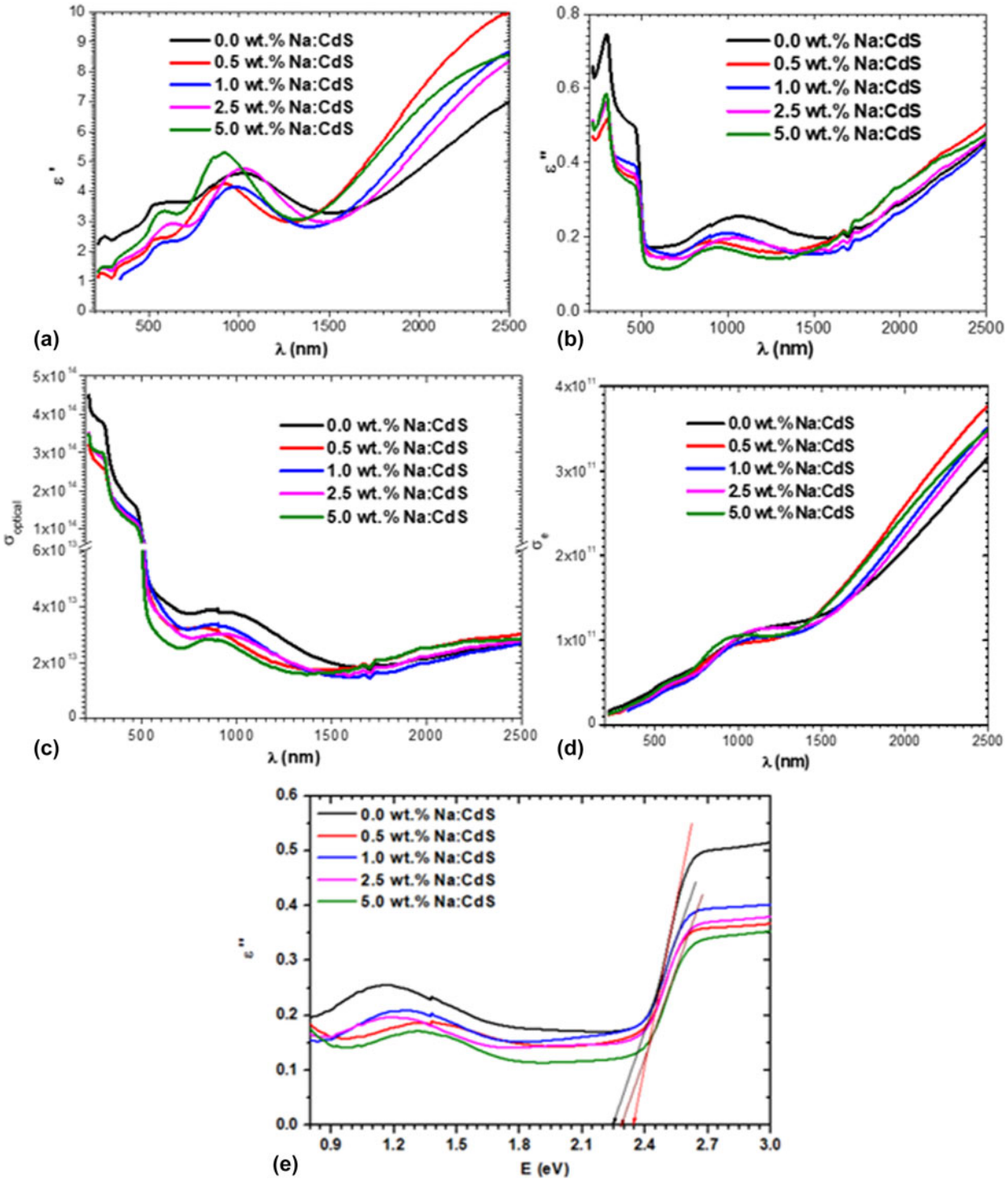

Figure 7: Plots of (a) dielectric constant, (b) dielectric loss, (c) optical conductivity, (d) electrical conductivity, and (e) optical dielectric loss versus phonon energy for $Na_xCd_{1-x}S$ films.

conductivities are also increasing linearly with the wavelength. The figure shows two such linear regions, below 1000 nm and above 1500 nm wavelengths. The values are almost uniform, 1000–1500 nm. However, the plot displays mixed tendency of electrical conductivity with Na content, and the pure sample has the maximum conductivity in the UV-Vis range, whereas at IR, above 1500 nm, it causes the least conductivity. Energy gap value was also determined from optical dielectric loss plot drawn as a function of energy in Fig. 7(e). It can be noticed that the energy gap values lie in range of 2.2–2.4 eV, which are in

quite agreement with energy gap values calculated by Tauc's plot in above. Similar type of calculation for energy gap using dielectric loss and Tauc's plot is reported earlier [38, 39].

NL optics

When a substantial intense light falls on a sample, the polarization (P) induced on it might not be described by a linear function of electric field (E), but rather requires a nonlinear relationship. Thus, the studies on the NL refractive index (n_2), and second and cubic order (NL) susceptibilities (χ^2 & χ^3) of the deposited thin films are of significance. The polarizability (P) in such condition contains a NL polarizability (P_{NL}) term, and could be expressed as [64]

$$P = \chi^1 E + P_{NL} \quad , \tag{11}$$

where χ^1 is the linear susceptibility and

$$P_{NL} = \chi^2 E^2 + \chi^3 E^3 \quad . \tag{12}$$

The values of χ^1 and χ^3 can be obtained from the linear refractive index (n_o) using [31, 65, 66, 67, 68].

$$\chi^1 = \frac{n_o^2 - 1}{4\pi} \quad , \tag{13}$$

and

$$\chi^3 = A(\chi^1)^4 = A\left(\frac{n_o^2 - 1}{4\pi}\right)^4 \quad , \tag{14}$$

with $A = 1.7 \times 10^{-10}$ esu [69].

Furthermore, the NL refractive index n_2 is related to χ^3 and n_o as [31, 69]

$$n_2 = \frac{12\pi\chi^3}{n_o} \quad . \tag{15}$$

Figures S1(a)–S1(c) (see Supplementary material) display the plots of linear, NL susceptibilities, and refractive index of the $Na_xCd_{1-x}S$ films. Both χ^1 and χ^3 first exhibit a decreasing tendency with the Na doping until 1 wt% $Na_xCd_{1-x}S$, beyond which it reverses the tendency, and the susceptibilities are found to be increasing with Na doping. The NL refractive plot has a close resemblance to the χ^3 plot in oscillating tendency but differs in terms of magnification and could be explained on the basis of linear relation between them. At high energy incident lights above 1.5 eV, the NL refractive index values of doped films are lower than that of pure CdS film, and the tendency is found to be initially decreasing with Na doping until 1 wt%, whereas 2.5 wt% and 5 wt% samples showed a gradual increasing tendency. This shows that the NL property of the refractive index can be reduced for the high energy incident beams and could be effectively utilized in optoelectronic device applications. The obtained nonlinear optical (NLO) parameters along with previous reports on pure/doped CdS/oxides films are tabulated in Table II for better comparison.

Optical limiting assessment

The optoelectronic field employs different kinds of optical detectors which are highly sensitive to the incident light and intensity. Often, it is required to protect these sensors from high power beams like lasers to avoid destruction, and hence the studies on optical limiting (OL) properties of the materials deserve special attention [57, 70, 71]. In the current work, we studied the OL properties of $Na_xCd_{1-x}S$ films against laser (λ = 650 nm) irradiation power of 15.07 mW. Table III lists the normalized outpower power of the transmitted laser beam. It was observed that the output power reduces with increase in sodium content and reaches up to 72.3% for 5 wt% $Na_xCd_{1-x}S$ sample. The reduction in the transmitted power could be attributed to the increase in the number of molecules in the doped samples [72, 73]. It can be seen that this reduction in the output power is gradual, and hence the prepared samples could be used for fine-tuning of the output power along with another steep reducing OL film.

Conclusion

Undoped and Na doped CdS thin films have been deposited by spray pyrolysis technique on glass substrates. XRD studies indicated that the $Na_xCd_{1-x}S$ films are grown in the hexagonal structure and crystallite sizes decreased with increasing Na doping wt%. The modification on the surface morphology of CdS thin films was revealed from SEM studies and are in agreement with XRD studies. Raman studies also confirmed wurtzite CdS structure with characteristic modes at 212 cm^{-1} having B_2 symmetry and 259 cm^{-1} with E_2 symmetry. The transmissions of the films are found to be dependent on Na doping wt% and increased from 45 to 60% for 5 wt% $Na_xCd_{1-x}S$ film. The band gap of the films first reduced because of the Na addition and then displayed a slight increase because of the reduced crystallite size. The refractive index values were estimated. Dielectric constant, dielectric loss, optical conductivity, and electrical conductivity analyses were made using optical data. The linear (χ^1) and NL (χ^3) optical susceptibility analyses of $Na_xCd_{1-x}S$ films showed a decreasing tendency with the Na doping until 1 wt% doping, above which it reversed this tendency and increased with Na doping. The NL refractive plot exhibited a close resemblance to that of χ^3 in oscillating tendency though differed in values. OL

TABLE II: Comparative NLO parameters reported for various films.

Authors	Materials	$\chi^{(1)}$	$\chi^{(3)}$ (esu)	n^2 (esu)
Khan et al. [74]	F:CdS	0.1–0.8	0.02×10^{-11} to 5.5×10^{-11}	1.8×10^{-12} to 6.1×10^{-10}
Shkir et al. [14]	Te:CdS	0.05–0.70	4×10^{-13} to 3.5×10^{-11}	2.4×10^{-14} to 5.5×10^{-10}
Shkir et al. [75]	Mg:ZnO	0.14–0.6	1.0×10^{-13} to 1.0×10^{-11}	2.0×10^{-13} to 1.5×10^{-10}
Khan et al. [76]	Ag:CdS	0.10–7.0	2.92×10^{-10} to 1×10^{-7}	1×10^{-9} to 2×10^{-7}
Radaf et al. [77]	F:CdS	...	1.74×10^{-12} to 16.6×10^{-12}	2.9×10^{-11} to 21.9×10^{-11}
Shkir et al. [13]	In:CdS	...	4.67×10^{-1} to 7.01×10^{-1}	2.14×10^{-7} to 4.99×10^{-7}
Arif et al. [78]	N:ZnO	0.3–9	1.0×10^{-11} to 1.0×10^{-8}	1.4×10^{-12} to 2.5×10^{-8}
Abrinaei et al. [79]	Al:ZnO	...	1.1×10^{-5} to 10.9×10^{-4}	-8.05×10^{-9} to 11.05×10^{-9}
Current work	Na:CdS	...	5.04×10^{-3} to 8.95×10^{-3}	3.17×10^{-8} to 6.28×10^{-8}

TABLE III: Optical limiting properties of $Na_xCd_{1-x}S$ films at $\lambda = 650$ nm.

	The input intensity, $I_o = 15.07$ mW	
Sample name	Output power, I (mW)	Normalized power % = $(I/I_o) \times 100$
0.0 wt% $Na_xCd_{1-x}S$	13.32	88.4
0.5 wt% $Na_xCd_{1-x}S$	12.60	83.6
1.0 wt% $Na_xCd_{1-x}S$	12.05	80.0
2.5 wt% $Na_xCd_{1-x}S$	11.40	75.6
5.0 wt% $Na_xCd_{1-x}S$	10.90	72.3

characteristics of the films were also studied using red laser at 650 nm wavelength. The results were promising for the systematic gradual decrease of intensity from 100 to 72% with doping for power regulating applications. However, owing to the gradual decrease, the samples are best suited for fine-tuning of the output power in conjunction with another steep reducing optical limiter.

Experimental section

Solution preparation for the deposition of $Na_xCd_{1-x}S$ thin films

0.025M $CdCl_2 \cdot H_2O$ and 0.025M $SC(NH_2)_2$ solutions prepared separately in 4:1 double distilled water (DDW) and ammonia under vigorous magnetic stirring were used as the precursor solutions and are acting as the sources of Cd^{2+} and S^{2-} ions, respectively. After mixing these solutions under magnetic stirring, separately prepared (0.0, 0.5, 1, 2.5, and 5 wt%) AR grade sodium sulfite (Na_2SO_3) aqueous solution in DDW was added to it as Na^+ dopant source to deposit (0.0, 0.5, 1, 2.5, and 5 wt%, respectively) Na-doped CdS thin films. Throughout the reactions, the pH of the solution was maintained at 11.5 using ammonia.

Film deposition using spray pyrolysis

Before film deposition, the glass substrates were thoroughly cleaned systematically using standard cleaning procedures. The spray pyrolysis method was followed at a maintained flow rate of 5 mL/min to deposit (0.0, 0.5, 1, 2.5, and 5 wt%) Na-doped CdS thin films, at a fixed substrate temperature of 300 °C and a substrate to spray nozzle distance of 0.27 m. The pressure of the carrier gas was about 1 kg/cm^2 [2]. After the deposition, the films were brought to RT naturally. An alpha Step profilometer was used to monitor the thicknesses of the films and obtained ~400 nm.

Thin film characterizations

Structural analysis of the films was made using a Shimadzu Lab-X- XRD-6000 diffractometer (at 40 kV and 30 mA) between the 2θ range 20–70°, at a speed of 4°/min. Elemental and morphological studies were made using JEOL JSM 6360 SEM/EDS unit (Japan). A Fisher Scientific DXR FT-Raman spectrometer was used for the Raman spectral studies, at $\lambda =$ 532 nm having 5 mW power. Optical measurements were carried out using a JASCO V-570 (Japan) UV–Vis–NIR spectrophotometer. PL emission measurements were done using a Lumina fluorescence spectrophotometer. OL properties of $Na_xCd_{1-x}S$ films were carried out using a red laser source ($\lambda = 650$ nm), with intensity = 15.07 mW.

Acknowledgments

Authors express their appreciation to the Deanship of Scientific Research at King Khalid University for funding this work through research groups program under grant number R.G.P. 2/41/40.

Supplementary material

To view supplementary material for this article, please visit https://doi.org/10.1557/jmr.2020.26.

References

1. **M.A. Islam, M.S. Hossain, M.M. Aliyu, P. Chelvanathan, Q. Huda, M.R. Karim, K. Sopian, and N. Amin**: Comparison of structural and optical properties of CdS thin films grown by CSVT, CBD and sputtering techniques. *Energy Procedia* **33**, 203 (2013).
2. **A. Tanushevski and H. Osmani**: CdS thin films obtained by chemical bath deposition in presence of fluorine and the effect of annealing on their properties. *Chalcogenide Lett.* **15**, 107 (2018).
3. **H. Moualkia, N. Attaf, L. Hadjeris, L. Herissi, and N. Abdelmalek**: *Preparation and Characterization of CdS Thin Films* (IEEE, Piscataway, New Jersey, US, 2012); p. 66.

4. **M. Ouafi, B. Jaber, L. Atourki, N. Zayyoun, A. Ihlal, A. Mzerd, and L. Laânab**: In situ low-temperature chemical bath deposition of CdS thin films without thickness limitation: Structural and optical properties. *Int. J. Photoenergy* **2018**, 1 (2018).
5. **F. Göde and S. Ünlü**: Synthesis and characterization of CdS window layers for PbS thin film solar cells. *Mater. Sci. Semicond. Process.* **90**, 92 (2019).
6. **J. Jie, W. Zhang, Y. Jiang, X. Meng, Y. Li, and S. Lee**: Photoconductive characteristics of single-crystal CdS nanoribbons. *Nano Lett.* **6**, 1887 (2006).
7. **W. Wondmagegn, I. Mejia, A. Salas-Villasenor, H. Stiegler, M. Quevedo-Lopez, R. Pieper, and B. Gnade**: CdS thin film transistor for inverter and operational amplifier circuit applications. *Microelectron. Eng.* **157**, 64 (2016).
8. **Y.L. Song, Y. Li, F.Q. Zhou, P.F. Ji, X.J. Sun, M.L. Wan, and M.L. Tian**: White electroluminescence from a prototypical light-emitting diode based on CdS/Si heterojunctions. *Mater. Lett.* **196**, 8 (2017).
9. **B-G. An, Y.W. Chang, H-R. Kim, G. Lee, M-J. Kang, J-K. Park, and J-C. Pyun**: Highly sensitive photosensor based on in situ synthesized CdS nanowires. *Sens. Actuators, B* **221**, 884 (2015).
10. **Y. Zhao, M. Yuan, Y. Chen, Y. Huang, J. Lian, S. Cao, H. Li, and L. Wu**: Size controllable preparation of sphere-based monolayer CdS thin films for white-light photodetectors. *Ceram. Int.* **44**, 2407 (2018).
11. **A.J. Khimani, S.H. Chaki, T.J. Malek, J.P. Tailor, S.M. Chauhan, and M.P. Deshpande**: Cadmium sulphide (CdS) thin films deposited by chemical bath deposition (CBD) and dip coating techniques—A comparative study. *Mater. Res. Express* **5**, 036406 (2018).
12. **S. Yılmaz, İ. Polat, M. Tomakin, T. Küçükömeroğlu, S.B. Töreli, and E. Bacaksız**: Sm-doped CdS thin films prepared by spray pyrolysis: A structural, optical, and electrical examination. *Appl. Phys. A* **124**, 502 (2018).
13. **M. Shkir, M. Anis, S.S. Shaikh, and S. AlFaify**: An investigation on structural, morphological, optical and third order nonlinear properties of facilely spray pyrolysis fabricated In:CdS thin films. *Superlattices Microstruct.* **133**, 106202 (2019).
14. **M. Shkir, S. Shaikh, and S. AlFaify**: An investigation on optical-nonlinear and optical limiting properties of CdS: An effect of Te doping concentrations for optoelectronic applications. *J. Mater. Sci.: Mater. Electron.* **30**, 17469 (2019).
15. **M. Shkir, I.M. Ashraf, S. AlFaify, A.M. El-Toni, M. Ahmed, and A. Khan**: A noticeable effect of Pr doping on key optoelectrical properties of CdS thin films prepared using spray pyrolysis technique for high-performance photodetector applications. *Ceram. Int.* **46**, 4652 (2019).
16. **M. Shkir, I.M. Ashraf, K.V. Chandekar, I.S. Yahia, A. Khan, H. Algarni, and S. AlFaify**: A significant enhancement in visible-light photodetection properties of chemical spray pyrolysis fabricated CdS thin films by novel Eu doping concentrations. *Sens. Actuators, A* **301**, 111749 (2020).
17. **M. Shkir, Z.R. Khan, M. Anis, S.S. Shaikh, and S. AlFaify**: A comprehensive study of opto-electrical and nonlinear properties of Cu@CdS thin films for optoelectronics. *Chin. J. Phys.* **63**, 51 (2020).
18. **G. Pandey, S. Dixit, and A.K. Shrivastava**: Effect of Gd^{3+} doping and reaction temperature on structural and optical properties of CdS nanoparticles. *Mater. Sci. Eng. B* **200**, 59 (2015).
19. **S. Agrawal and A. Khare**: Effect of La on optical and structural properties of CdS–Se films. *Arabian J. Chem.* **8**, 450 (2015).
20. **M.A. Khalid and H.A. Jassem**: Electrical and optical properties of polycrystalline Ag-doped CdS thin films. *Acta Phys. Hung.* **73**, 29 (1993).
21. **J.A. Dávila-Pintle, R. Lozada-Morales, M.R. Palomino-Merino, J.A. Rivera-Márquez, O. Portillo-Moreno, and O. Zelaya-Angel**: Electrical properties of Er-doped CdS thin films. *J. Appl. Phys.* **101**, 013712 (2007).
22. **L. Karimi, M.E. Yazdanshenas, R. Khajavi, A. Rashidi, and M. Mirjalili**: Using graphene/TiO_2 nanocomposite as a new route for preparation of electroconductive, self-cleaning, antibacterial and antifungal cotton fabric without toxicity. *Cellulose* **21**, 3813 (2014).
23. **M. Sreenivas, G.S. Harish, and P.S. Reddy**: Synthesis and Raman studies of Ce doped Cds nanoparticles. *Int. J. Adv. Res.* **2**, 468 (2014).
24. **S. Mageswari, L. Dhivya, B. Palanivel, and R. Murugan**: Structural, morphological and optical properties of Na and K dual doped CdS thin film. *J. Alloys Compd.* **545**, 41 (2012).
25. **M.J. Iqbal Khan and Z. Kanwal**: Investigation of optical properties of CdS for various Na concentrations for nonlinear optical applications (A DFT study). *Optik* **193**, 162985 (2019).
26. **M. Shkir and S. AlFaify**: Tailoring the structural, morphological, optical and dielectric properties of lead iodide through Nd^{3+} doping. *Sci. Rep.* **7**, 16091 (2017).
27. **M.A. Manthrammel, A. Fatehmulla, A.M. Al-Dhafiri, A.S. Alshammari, and A. Khan**: Temperature dependent surface and spectral modifications of nano V_2O_5 films. *Opt. Spectrosc.* **122**, 420 (2017).
28. **M. Shkir, M. Arif, V. Ganesh, M.A. Manthrammel, A. Singh, S.R. Maidur, P.S. Patil, I.S. Yahia, H. Algarni, and S. AlFaify**: Linear, third order nonlinear and optical limiting studies on MZO/FTO thin film system fabricated by spin coating technique for electro-optic applications. *J. Mater. Res.* **33**, 3880 (2018).
29. **M.A. Manthrammel, V. Ganesh, M. Shkir, I.S. Yahia, and S. Alfaify**: Facile synthesis of La-doped CdS nanoparticles by microwave assisted co-precipitation technique for optoelectronic application. *Mater. Res. Express* **6**, 025022 (2018).
30. **M. Shkir, I.S. Yahia, M. Kilany, M.M. Abutalib, S. AlFaify, and R. Darwish**: Facile nanorods synthesis of KI:HAp and their structure-morphology, vibrational and bioactivity analyses for biomedical applications. *Ceram. Int.* **45**, 50 (2019).

31. **V. Ganesh, I. Yahia, S. AlFaify, and M. Shkir**: Sn-doped ZnO nanocrystalline thin films with enhanced linear and nonlinear optical properties for optoelectronic applications. *J. Phys. Chem. Solids* **100**, 115 (2017).
32. **M. Gilic, J. Trajic, N. Romcevic, M. Romcevic, D.V. Timotijevic, G. Stanisic, and I.S. Yahia**: Optical properties of CdS thin films. *Opt. Mater.* **35**, 1112 (2013).
33. **M.V. Malashchonak, A.V. Mazanik, O.V. Korolik, E.A. Streltsov, and A.I. Kulak**: Influence of wide band gap oxide substrates on the photoelectrochemical properties and structural disorder of CdS nanoparticles grown by the successive ionic layer adsorption and reaction (SILAR) method. *Beilstein J. Nanotechnol.* **6**, 2252 (2015).
34. **V.M. Dzhagan, M.Y. Valakh, C. Himcinschi, A.G. Milekhin, D. Solonenko, N.A. Yeryukov, O.E. Raevskaya, O.L. Stroyuk, and D.R.T. Zahn**: Raman and infrared phonon spectra of ultrasmall colloidal CdS nanoparticles. *J. Phys. Chem.* **118**, 19492 (2014).
35. **M.A. Nusimovici, M. Balkanski, and J.L. Birman**: Lattice dynamics of wurtzite: CdS. II. *Phys. Rev. B* **1**, 595 (1970).
36. **M. Shkir and S. AlFaify**: Effect of Gd^{3+} doping on structural, morphological, optical, dielectric, and nonlinear optical properties of high-quality PbI_2 thin films for optoelectronic applications. *J. Mater. Res.* **34**, 2765 (2019).
37. **M. Shkir, A. Khan, A.M. El-Toni, A. Aldalbahi, I.S. Yahia, and S. AlFaify**: Structural, morphological, opto-nonlinear-limiting studies on Dy:PbI_2/FTO thin films derived facilely by spin coating technique for optoelectronic technology. *J. Phys. Chem. Solids* **130**, 189 (2019).
38. **S.B. Aziz, A.Q. Hassan, S.J. Mohammed, W.O. Karim, M. Kadir, H. Tajuddin, and N. Chan**: Structural and optical characteristics of PVA: C-dot composites: Tuning the absorption of ultra violet (UV) region. *Nanomaterials* **9**, 216 (2019).
39. **S.B. Aziz, R.B. Marif, M. Brza, A.N. Hassan, H.A. Ahmad, Y.A. Faidhalla, and M. Kadir**: Structural, thermal, morphological and optical properties of PEO filled with biosynthesized Ag nanoparticles: New insights to band gap study. *Results Phys.* **13**, 102220 (2019).
40. **S.B. Aziz, S.M. Mamand, S.R. Saed, R.M. Abdullah, and S.A. Hussein**: New method for the development of plasmonic metal-semiconductor interface layer: Polymer composites with reduced energy band gap. *J. Nanomater.* **2017**, 1 (2017).
41. **R.M. Abdullah, S.B. Aziz, S.M. Mamand, A.Q. Hassan, S.A. Hussein, and M. Kadir**: Reducing the crystallite size of spherulites in PEO-based polymer nanocomposites mediated by carbon nanodots and Ag nanoparticles. *Nanomaterials* **9**, 874 (2019).
42. **S.B. Aziz, H.M. Ahmed, A.M. Hussein, A.B. Fathulla, R.M. Wsw, and R.T. Hussein**: Tuning the absorption of ultraviolet spectra and optical parameters of aluminum doped PVA based solid polymer composites. *J. Mater. Sci.: Mater. Electron.* **26**, 8022 (2015).
43. **S. Aziz, M. Rasheed, and H. Ahmed**: Synthesis of polymer nanocomposites based on [methyl cellulose]$_{(1-x)}$:$(CuS)_x$ (0.02 M $\leq x \leq$ 0.08 M) with desired optical band gaps. *Polymers* **9**, 194 (2017).
44. **M. Brza, S.B. Aziz, H. Anuar, and M.H.F. Al Hazza**: From green remediation to polymer hybrid fabrication with improved optical band gaps. *Int. J. Mol. Sci.* **20**, 3910 (2019).
45. **B.D. Viezbicke, S. Patel, B.E. Davis, and D.P. Birnie**: Evaluation of the tauc method for optical absorption edge determination: ZnO thin films as a model system. *Phys. Status Solidi B* **252**, 1700 (2015).
46. **A. Bedia, F.Z. Bedia, M. Aillerie, N. Maloufi, and B. Benyoucef**: Influence of the thickness on optical properties of sprayed ZnO hole-blocking layers dedicated to inverted organic solar cells. *Energy Procedia* **50**, 603 (2014).
47. **J. Lv, K. Huang, X. Chen, J. Zhu, C. Cao, X. Song, and Z. Sun**: Optical constants of Na-doped ZnO thin films by sol–gel method. *Opt. Commun.* **284**, 2905 (2011).
48. **İ. Polat**: Effects of Na-doping on the efficiency of ZnO nanorods-based dye sensitized solar cells. *J. Mater. Sci.: Mater. Electron.* **25**, 3721 (2014).
49. **M.M. Aslam, S.M. Ali, A. Fatehmulla, W.A. Farooq, M. Atif, A.M. Al-Dhafiri, and M.A. Shar**: Growth and characterization of layer by layer CdS–ZnS QDs on dandelion like TiO_2 microspheres for QDSSC application. *Mater. Sci. Semicond. Process.* **36**, 57 (2015).
50. **P.P. Hankare, P.A. Chate, and D.J. Sathe**: CdS thin film: Synthesis and characterization. *Solid State Sci.* **11**, 1226 (2009).
51. **S. Yılmaz, İ. Polat, M. Tomakin, and E. Bacaksız**: A research on growth and characterization of CdS:Eu thin films. *Appl. Phys. A* **125**, 67 (2019).
52. **S. Yılmaz, İ. Polat, M. Tomakin, and E. Bacaksız**: Determination of optimum Er-doping level to get high transparent and low resistive $Cd_{1-x}Er_xS$ thin films. *J. Mater. Sci.: Mater. Electron.* **30**, 5662 (2019).
53. **S. Yılmaz, Y. Atasoy, M. Tomakin, and E. Bacaksız**: Comparative studies of CdS, CdS:Al, CdS:Na, and CdS:(Al–Na) thin films prepared by spray pyrolysis. *Superlattices Microstruct.* **88**, 299 (2015).
54. **R. Kumar, R. Das, M. Gupta, and V. Ganesan**: Compositional effect of antimony on structural, optical, and photoluminescence properties of chemically deposited $(Cd_{1-x}Sb_x)S$ thin films. *Superlattices Microstruct.* **59**, 29 (2013).
55. **S.J. Ikhmayies and R.N. Ahmad-Bitar**: Dependence of the photoluminescence of CdS:In thin films on the excitation power of the laser. *J. Lumin.* **149**, 240 (2014).
56. **G. Murali, D. Amaranatha Reddy, G. Giribabu, R.P. Vijayalakshmi, and R. Venugopal**: Room temperature ferromagnetism in Mn doped CdS nanowires. *J. Alloys Compd.* **581**, 849 (2013).
57. **M. Aslam Manthrammel, A.M. Aboraia, M. Shkir, I.S. Yahia, M.A. Assiri, H.Y. Zahran, V. Ganesh, S. AlFaify, and**

A.V. Soldatov: Optical analysis of nanostructured rose bengal thin films using Kramers–Kronig approach: New trend in laser power attenuation. *Opt. Laser Technol.* **112**, 207 (2019).

58. **S.B. Aziz, M.A. Rasheed, A.M. Hussein, and H.M. Ahmed**: Fabrication of polymer blend composites based on $[PVA\text{-}PVP]_{(1-x)}:(Ag_2S)_x$ $(0.01 \leq x \leq 0.03)$ with small optical band gaps: Structural and optical properties. *Mater. Sci. Semicond. Process.* **71**, 197 (2017).
59. **S. Aziz**: Morphological and optical characteristics of $chitosan_{(1-x)}:Cu^{o}_{x}$ $(4 \leq x \leq 12)$ based polymer nano-composites: Optical dielectric loss as an alternative method for tauc's model. *Nanomaterials* **7**, 444 (2017).
60. **K.S. Ojha and R.L. Srivastava**: Dielectric and impedance study of optimized cadmium sulphide thin film. *Chalcogenide Lett.* **10**, 1 (2013).
61. **M.A. Assiri, M. Aslam Manthrammel, A.M. Aboraia, I.S. Yahia, H.Y. Zahran, V. Ganesh, M. Shkir, S. AlFaify, and A.V. Soldatov**: Kramers–Kronig calculations for linear and nonlinear optics of nanostructured methyl violet (CI-42535): New trend in laser power attenuation using dyes. *Phys. B Condens. Matter* **552**, 62 (2019).
62. **H.S. Bolarinwa, M.U. Onuu, A.Y. Fasasi, S.O. Alayande, L.O. Animasahun, I.O. Abdulsalami, O.G. Fadodun, and I.A. Egunjobi**: Determination of optical parameters of zinc oxide nanofibre deposited by electrospinning technique. *Journal of Taibah University for Science* **11**, 1245 (2017).
63. **M.M. El-Desoky, G.A. El-Barbary, D.E. El Refaey, and F. El-Tantawy**: Optical constants and dispersion parameters of La-doped ZnS nanocrystalline films prepared by sol–gel technique. *Optik* **168**, 764 (2018).
64. **M. Frumar, J. Jedelský, B. Frumarova, T. Wagner, and M. Hrdlička**: Optically and thermally induced changes of structure, linear and non-linear optical properties of chalcogenides thin films. *J. Non-Cryst. Solids* **326**, 399 (2003).
65. **H. Ticha and L. Tichy**: Semiempirical relation between non-linear susceptibility (refractive index), linear refractive index and optical gap and its application to amorphous chalcogenides. *J. Optoelectron. Adv. Mater.* **4**, 381 (2002).
66. **C.C. Wang**: Empirical relation between the linear and the third-order nonlinear optical susceptibilities. *Phys. Rev. B* **2**, 2045 (1970).
67. **J. Wynne**: Nonlinear optical spectroscopy of χ^3 in $LiNbO_3$. *Phys. Rev. Lett.* **29**, 650 (1972).
68. **V. Ganesh, M. Shkir, S. AlFaify, I. Yahia, H. Zahran, and A.A. El-Rehim**: Study on structural, linear and nonlinear optical properties of spin coated N doped CdO thin films for optoelectronic applications. *J. Mol. Struct.* **1150**, 523 (2017).
69. **D. Hanna**: *Handbook of Laser Science and Technology*, **35**, 12 (Journal of Modern Optics, 1988).
70. **L.W. Tutt and A. Kost**: Optical limiting performance of C60 and C70 solutions. *Nature* **356**, 225 (1992).
71. **G.L. Wood, W.W. Clark, M.J. Miller, G.J. Salamo, and E.J. Sharp**: Evaluation of passive optical limiters and switches. In *Materials for Optical Switches, Isolators, and Limiters*, vol. **1105** (International Society for Optics and Photonics, 1989); p. 154. https://doi.org/10.1117/12.960622 Event: SPIE 1989 Technical Symposium on Aerospace Sensing, 1989, Orlando, FL, USA.
72. **L.G. Holmen and M.W. Haakestad**: Optical limiting properties and z-scan measurements of carbon disulfide at 2.05 μm wavelength. *J. Opt. Soc. Am. B* **33**, 1655 (2016).
73. **P. Poornesh, P.K. Hegde, G. Umesh, M. Manjunatha, K. Manjunatha, and A. Adhikari**: Nonlinear optical and optical power limiting studies on a new thiophene-based conjugated polymer in solution and solid PMMA matrix. *Opt. Laser Technol.* **42**, 230 (2010).
74. **Z.R. Khan, M. Shkir, V. Ganesh, S. AlFaify, I.S. Yahia, and H.Y. Zahran**: Linear and nonlinear optics of CBD grown nanocrystalline F doped CdS thin films for optoelectronic applications: An effect of thickness. *J. Electron. Mater.* **47**, 5386 (2018).
75. **M. Shkir, M. Arif, V. Ganesh, M.A. Manthrammel, A. Singh, I.S. Yahia, S.R. Maidur, P.S. Patil, and S. AlFaify**: Investigation on structural, linear, nonlinear and optical limiting properties of sol–gel derived nanocrystalline Mg doped ZnO thin films for optoelectronic applications. *J. Mol. Struct.* **1173**, 375 (2018).
76. **Z.R. Khan, M. Shkir, A.S. Alshammari, V. Ganesh, S. AlFaify, and M. Gandouzi**: Structural, linear and third order nonlinear optical properties of sol–gel grown Ag–CdS nanocrystalline thin films. *J. Electron. Mater.* **48**, 1122 (2019).
77. **I. El Radaf, T.A. Hameed, and I. Yahia**: Synthesis and characterization of F-doped CdS thin films by spray pyrolysis for photovoltaic applications. *Mater. Res. Express* **5**, 066416 (2018).
78. **M. Arif, M. Shkir, S. AlFaify, A. Sanger, P.M. Vilarinho, and A. Singh**: Linear and nonlinear optical investigations of N:ZnO/ITO thin films system for opto-electronic functions. *Opt. Laser Technol.* **112**, 539 (2019).
79. **F. Abrinaei and M. Shirazi**: Nonlinear optical investigations on Al doping ratio in ZnO thin film under pulsed Nd:YAG laser irradiation. *J. Mater. Sci.: Mater. Electron.* **28**, 17541 (2017).